



<sup>6</sup>US Forest Service, Rocky Mountain Research Station, Fire Sciences Laboratory, Missoula, MT, USA

<sup>7</sup>University of Alcalá, Department of Geography, Calle Colegios 2, Alcalá de Henares 28801, Spain

<sup>8</sup>IRD, UMR CEFE, 1919 route de mende, 34293 Montpellier Cedex 5, France

<sup>9</sup>College of Engineering, Mathematics and Physical Sciences, University of Exeter, EX4 4QE, UK

Received: 15 February 2014 – Accepted: 20 March 2014 – Published: 10 April 2014

Correspondence to: C. Yue (chao.yue@lsce.ipsl.fr)

Published by Copernicus Publications on behalf of the European Geosciences Union.

## GMDD

7, 2377–2427, 2014

### Modelling global burned area and fire regime

C. Yue et al.

Title Page

Abstract

Introduction

Conclusions

References

Tables

Figures

⏪

⏩

◀

▶

Back

Close

Full Screen / Esc

Printer-friendly Version

Interactive Discussion



## Abstract

Fire is an important global ecological process that determines the distribution of biomes, with consequences for carbon, water, and energy budgets. The modelling of fire is critical for understanding its role in both historical and future changes in terrestrial ecosystems and the climate system. This study incorporates the process-based prognostic fire module SPITFIRE into the global vegetation model ORCHIDEE, which was then used to simulate the historical burned area and the fire regime for the 20th century. For 2001–2006, the simulated global spatial extent of fire occurrence agrees well with that given by the satellite-derived burned area datasets (L3JRC, GLOB-CARBON, GFED3.1) and captures 78–92% of global total burned area depending on which dataset is used for comparison. The simulated global annual burned area is 329 Mha yr<sup>-1</sup>, which falls within the range of 287–384 Mha yr<sup>-1</sup> given by the three global observation datasets and is close to the 344 Mha yr<sup>-1</sup> given by GFED3.1 data when crop fires are excluded. The simulated long-term trends of burned area agree best with the observation data in regions where fire is mainly driven by the climate variation, such as boreal Russia (1920–2009), and the US state of Alaska and Canada (1950–2009). At the global scale, the simulated decadal fire trend over the 20th century is in moderate agreement with the historical reconstruction, possibly because of the uncertainties of past estimates, and because land-use change fires and fire suppression are not explicitly included in the model. Over the globe, the size of large fires (the 95th quantile fire size) is systematically underestimated by the model compared with the fire patch data as reconstructed from MODIS 500 m burned area data. Two case studies of fire size distribution in boreal North America and southern Africa indicate that both the number and the size of big fires are underestimated, which could be related with too low fire spread rate (in the case of static vegetation) and fire duration time. Future efforts should be directed towards building consistent spatial observation datasets for key parameters of the model in order to constrain the model error at each key step of the fire modelling.

## Modelling global burned area and fire regime

C. Yue et al.

Title Page

Abstract

Introduction

Conclusions

References

Tables

Figures



Back

Close

Full Screen / Esc

Printer-friendly Version

Interactive Discussion



## 1 Introduction

Fire is an important process in the Earth system, that existed long before the large-scale appropriation of natural ecosystems by humans (Bowman et al., 2009; Daniiau et al., 2013). Fires have multiple biophysical and ecological consequences, and they are also an important source of atmospheric trace gases and aerosol particles (Langmann et al., 2009; van der Werf et al., 2010). By damaging some plant types and concurrently promoting others, fires play an important role in shaping vegetation structure and function (Bond et al., 2005; Pausas and Keeley, 2009). Fire changes the surface albedo, aerodynamic roughness, and the sensible and latent heat fluxes; fire-induced ecosystem change may thus influence the surface energy budget, and in turn the boundary-layer climate (Beck et al., 2011; Randerson et al., 2006; Rogers et al., 2013). Further, gas and aerosol species emitted to the atmosphere from biomass burning modify atmospheric composition and the radiative forcing balance (Tosca et al., 2013; Ward et al., 2012). Fire aerosols also degrade air quality and cause increased health risk (Marlier et al., 2013). Thus mechanistic inclusion of fire processes and the resultant emissions in Earth system models is needed, in order to investigate the role of fire in past, present and future biophysical and biogeochemical processes.

The type of fire model embedded in global vegetation models has evolved from simple fire hazard models (Thonicke et al., 2001) to the current state-of-the-art process-based fire models (Kloster et al., 2010; Li et al., 2012; Thonicke et al., 2010). These latter fire models explicitly simulate ignition from both natural and human sources, and fire propagation, fuel combustion and fire mortality processes, ideally at daily or even finer time steps. Evaluation of fire models in previous studies using global land surface models (Li et al., 2012; Prentice et al., 2011) has mainly focused on the models' skill in broadly reproducing the large-scale distribution of fire activity during the past decade using global satellite observations. Less attention has been paid to the simulation of long-term historical fire trend, and fire regimes, including the number, size

GMDD

7, 2377–2427, 2014

### Modelling global burned area and fire regime

C. Yue et al.

Title Page

Abstract

Introduction

Conclusions

References

Tables

Figures

◀

▶

◀

▶

Back

Close

Full Screen / Esc

Printer-friendly Version

Interactive Discussion



and intensity of fires – essential variables governing fire-climate-vegetation feedbacks (Archibald et al., 2013; Barrett et al., 2011; Hoffmann et al., 2012).

It is well known that across all fire-prone ecosystems of the globe, the magnitude and trend of burned area are driven by large and infrequent fire events (Kasischke and Turetsky, 2006; Keeley et al., 1999; Stocks et al., 2002). These large fires have profound impacts on landscape heterogeneity (Schoennagel et al., 2008; Turner et al., 1994) and biological diversity (Burton et al., 2008) and may also produce a higher rate of carbon emissions compared to small fires (Kasischke and Hoy, 2012). In some ecosystems, past climate warming is documented to have increased the occurrence of large fires (Kasischke et al., 2010; Westerling et al., 2006), and fire regimes are projected to evolve with future climate change (Westerling et al., 2011). Given the importance of these big fires, it is essential that we should evaluate the ability of fire models to simulate their occurrence.

In this study, we have incorporated the SPITFIRE fire model (Thonicke et al., 2010) into the global land surface model ORCHIDEE (Krinner et al., 2005). This has allowed us to simulate global fire activity during the 20th century, and to perform an in-depth model evaluation of burned area, and fire regime, including fire numbers and fire size. The present study focuses on evaluating the model's performance at simulating the processes of ignition, fire size distribution and burned area. Quantification of fire CO<sub>2</sub> emission as a component of the terrestrial carbon balance will be presented in a companion paper (Part 2). Specifically, the objectives of the present study are: (1) to evaluate the simulated burned area using multiple datasets including satellite-derived burned area data, government fire agency survey data, and historical reconstruction of burned area over the 20th century (Sects. 3.1, 3.2, 3.3, 3.4 and 3.5); (2) to compare the simulated fire size distribution to observations in order to investigate the model's ability to simulate the occurrence of large fires (Sect. 3.6); (3) to evaluate the simulated fire regimes for the large fires (the 95th quantile fire intensity, the 95th quantile fire size) (Sect. 3.7); and (4) to investigate the potential sources of error in the model in order to identify the need for future research and potential model improvements (Sect. 4.2).

Modelling global  
burned area and fire  
regime

C. Yue et al.

Title Page

Abstract

Introduction

Conclusions

References

Tables

Figures



Back

Close

Full Screen / Esc

Printer-friendly Version

Interactive Discussion



## 2 Data and methods

### 2.1 Model description

The processes and equations of the fire model SPITFIRE, as described by Thonicke et al. (2010), were implemented in the vegetation model ORCHIDEE (Krinner et al., 2005). The SPITFIRE model operates on a daily time step, consistent with the STOMATE sub-module in ORCHIDEE, which simulates vegetation carbon cycle processes (photosynthates allocation, litterfall, litter and soil carbon decomposition). The major processes within SPITFIRE are briefly described below with applicable minor modifications (see Thonicke et al., 2010 for more detailed information).

1. *Potential ignition* includes ignitions by both lightning and human activity. Remotely sensed lightning flash counts (Cecil et al., 2012) were obtained from the High Resolution Monthly Climatology of lightning flashes by the Lightning Imaging Sensor–Optical Transient Detector (LIS/OTD) ([http://gcmd.nasa.gov/records/GCMD\\_lohrmc.html](http://gcmd.nasa.gov/records/GCMD_lohrmc.html)). The LIS/OTD dataset provides annual mean flash rate over the period of 1995–2000 on a  $0.5^\circ$  grid with a monthly time step. This annual data was used each year throughout the simulation. Following Prentice et al. (2011), the proportion of lightning flashes that reach the ground with sufficient energy to ignite a fire is taken as 0.03. This value differs from that in the original SPITFIRE model as implemented in LPJ-DGVM (Thonicke et al., 2010); there a cloud-to-ground (CG) flashing ratio of 0.2 was used, followed by a further ignition efficiency of 0.04.

To estimate potential ignitions by humans, the original Eqs. (3) and (4) in Thonicke et al. (2010) were modified for the purpose of unit adjustment, as below:

$$I_H = PD \times 30.0 \times e^{-0.5 \times \sqrt{PD}} \times a(\text{ND}) / 10\,000 \quad (1)$$

where  $I_H$  is the daily ignition number ( $1 \text{ day}^{-1} \text{ km}^{-2}$ ), PD is population density (individuals  $\text{km}^{-2}$ ). The parameter  $a(\text{ND})$  (ignitions individual $^{-1} \text{ day}^{-1}$ ) represents the

## GMDD

7, 2377–2427, 2014

### Modelling global burned area and fire regime

C. Yue et al.

Title Page

Abstract

Introduction

Conclusions

References

Tables

Figures

◀

▶

◀

▶

Back

Close

Full Screen / Esc

Printer-friendly Version

Interactive Discussion



propensity of people to produce ignition events; it is a spatially explicit parameter in the Thonicke et al. (2010) LPJ-DGVM implementation, but following Venevsky et al. (2002),  $a(\text{ND})$  is assumed to be a global constant of 0.22 in our simulation.

The spatial distribution of  $a(\text{ND})$  used by Thonicke et al. (2010) is given in Supplement Fig. S1. The  $a(\text{ND})$  values for many regions are within 50% of the uniform value used here, although northern Australia is an exception. Test simulations showed that using a uniform  $a(\text{ND})$  value rather than the original spatial dataset has little influence on the simulated regional burned area (see Supplement Fig. S2).

2. *Fire numbers* are derived by scaling the potential ignitions (which include both human and lightning ignitions) using the fire danger index (FDI), which is derived by comparing the simulated daily fuel moisture to a Plant Functional Type (PFT) dependent moisture of extinction. All fires with a fireline intensity lower than  $50 \text{ kW m}^{-1}$  are assumed unable to propagate and therefore are suppressed as stated by Thonicke et al. (2010).
3. *Mean fire size* is calculated by assuming an elliptical shape of fire, with the major axis length being the product of fire spread rate and fire duration time. Fire spread rate is obtained using the Rothermel equation (Rothermel, 1972; Wilson, 1982). Fire duration time is modelled to increase as a logistic curve with fire danger index, with a maximum duration of 241 min (4 h).
4. *Daily burned area* is calculated each day as the product of daily fire number and the mean fire size.
5. *Fire-induced tree mortality* is determined from both crown and cambial damage by fire. Crown damage depends on the fraction of tree crown that is affected by crown scorch, which further depends on tree crown length, tree height and the fire flame height. Fire flame height is derived from surface fire intensity. The cambial

## Modelling global burned area and fire regime

C. Yue et al.

Title Page

Abstract

Introduction

Conclusions

References

Tables

Figures

◀

▶

◀

▶

Back

Close

Full Screen / Esc

Printer-friendly Version

Interactive Discussion





## Modelling global burned area and fire regime

C. Yue et al.

Title Page

Abstract

Introduction

Conclusions

References

Tables

Figures

◀

▶

◀

▶

Back

Close

Full Screen / Esc

Printer-friendly Version

Interactive Discussion



The equations for surface fuel combustion completeness given by Thonicke et al. (2010) follow Peterson and Ryan (1986), which allow combustion completeness to decrease with increasing fuel wetness and level out when fuel wetness drops below a threshold (Fig. 1). During model testing, we found that because fuel wetness frequently approaches zero, the simulated fuel combustion completeness is much higher than the field experiment values reported by van Leeuwen et al. (2014), who compiled the combustion completeness measurements for fires in different biomes across the globe. We therefore modified the maximum combustion completeness for fuel classes of 100 h and 1000 h to be the same as the mean combustion completeness compiled by van Leeuwen et al. (2014). This biome-dependent maximum combustion completeness is 0.48 for tropical broadleaf evergreen and seasonal forests, 0.45 for temperate forest, 0.41 for boreal forest, 0.85 for grassland, and 0.35 for agricultural land.

### 2.3 Input dataset and the simulation protocol

The six-hourly climate fields used to drive the model were from the CRU-NCEP dataset ([http://dods.extra.cea.fr/store/p529viov/cruncep/V4\\_1901\\_2012/readme.htm](http://dods.extra.cea.fr/store/p529viov/cruncep/V4_1901_2012/readme.htm)). Population density for the 20th century was retrieved from the History Database of the Global Environment (HYDE) as compiled by the Netherlands Environmental Assessment Agency (<http://themasites.pbl.nl/tridion/en/themasites/hyde/download/index-2.html>). From 1850 till 2005, the HYDE gridded data are available for the beginning of each decade and for 2005. Annual data were linearly interpolated within each decade, and further re-gridded to 0.5° resolution. For 2006–2009, population density was set constant at the 2005 value.

A three-step simulation protocol was used. For the first two steps, the atmospheric CO<sub>2</sub> was fixed at the pre-industrial level (285 ppm) and the climate forcing data of 1901–1930 were repeated in loop. The first step was a without-fire spin-up from bare ground lasting for 200 years (including a 3000-year run of soil-only processes to speed up the equilibrium of mineral soil carbon). The second step was a fire-disturbed spin-up lasting for 150 years, with fire being switched on to account for fire disturbances in the

pre-industrial era. Fire ignitions from human activity were included in the fire-disturbed spin-up, with the human population density being fixed at 1850 level. This procedure assumes that the model reached an equilibrium state under conditions of pre-industrial atmospheric CO<sub>2</sub> and climate.

5 The third step was a transient simulation from 1850 to 2009 with increasing atmospheric CO<sub>2</sub>, climate change, and varying human population density. The climate data used for the transient simulation of 1850–1900 are a repeat of 1901–1910, for the sake of stability. Before entering the transient simulation, the mineral soil carbon stock was verified to vary within 0.1 % (with a slight global carbon sink of 0.13 PgCyr<sup>-1</sup>, and a negligible annual trend of 0.003 PgCyr<sup>-1</sup> during the last 50  
10 years of the fire-disturbed spin-up excluding all crops, for which fires are not simulated). For the current simulation, the vegetation dynamics module of ORCHIDEE was turned off, i.e., the simulation used a static current-day vegetation distribution map (converted into the 13-PFT map in ORCHIDEE based on the IGBP 1 km vegetation map,  
15 http://webmap.ornl.gov/wcsdown/dataset.jsp?ds\_id=930), and no land-cover change was included.

Agricultural fires are not simulated in ORCHIDEE, even though the model has two PFTs that approximately represent C3 and C4 crops (but without realistic species-specific phenology). Magi et al. (2012) show that agricultural fire seasons differ significantly from those of natural fires, warranting a special treatment of agricultural fires  
20 in global fire modelling (Li et al., 2012). Agricultural fires make up a rather small proportion of the total global amount in terms of both burned area (4.3% according to the GFED3.1 dataset) and carbon emissions (less than 2% according to GFED3.1). Further, deforestation fires are not explicitly simulated. Evidences show that deforestation  
25 fires occur during the “time window” when climate is dry enough to allow complete burning (van der Werf et al., 2008a). The simulated fire danger index should partly capture this fire climate window, and that the model is able to account for some “deforestation” fire activity in tropical and subtropical forests, but not all, because our land cover map is static.

## Modelling global burned area and fire regime

C. Yue et al.

Title Page

Abstract

Introduction

Conclusions

References

Tables

Figures



Back

Close

Full Screen / Esc

Printer-friendly Version

Interactive Discussion



## 2.4 Datasets used to evaluate model performance

Several datasets were prepared and used to compare simulated burned area and fire regime with global Earth observations and government fire agency survey data.

### 2.4.1 Spatially gridded burned area data

#### 5 Satellite-derived burned area data

The *GFED3.1* fire carbon emission dataset provides monthly burned area data at 0.5° resolution for 1997–2009 with global coverage (Giglio et al., 2010). The GFED3.1 data were mainly generated using MODIS imagery with additional images from TRMM IRS and ERS ATSR. The fire carbon emissions data were also provided which are model simulation results by applying the CASA model (van der Werf et al., 2010).

*L3JRC* dataset provides daily global burned area data at 1 km resolution for April 2000 to March 2007; these data were generated from the 1 km SPOT VEGETATION satellite imagery (Tansey et al., 2008). This dataset was assembled at 0.5° resolution at monthly time step for use in the present study.

*GLOBCARBON* burned area dataset was produced from a combination of SPOT VEGETATION and ERS2–ATSR2/ENVISAT AATSR data as one of the four land products of the ESA GLOBCARBON initiative (Plummer et al., 2007). Global burned area data were provided at monthly resolution with four different spatial resolutions (1 km/10 km/0.25°/0.5°) covering 1998–2007.

#### 20 Historical burned area reconstruction for the 20th century

To evaluate the simulated burned area for the 20th century, historical burned area data were used. These data, which cover the period 1900–2000, were compiled by Mouillot and Field (2005) at 1° resolution and monthly time step (hereafter referred to as the Mouillot data). The data were generated by first synthesizing the burned area information from published data at national or regional scale for the periods of the 1980s

## Modelling global burned area and fire regime

C. Yue et al.

Title Page

Abstract

Introduction

Conclusions

References

Tables

Figures



Back

Close

Full Screen / Esc

Printer-friendly Version

Interactive Discussion



or 1990s, further interpolated spatially at the global scale at 1° resolution using the available satellite-derived active fire distribution. Then national fire statistics, historical land-use practices and other fire-relevant quantitative information (such as tree ring reconstruction) were used to build the historical fire temporal trend to interpolate historical burned area.

When comparing the burned area given by GFED3.1 and the Mouillot data for their overlapping period of 1997–2000, the global total burned area given by Mouillot and Field (2005) is 52 % higher than GFED3.1 with significant regional discrepancies. As the satellite-derived data is considered to be more reliable than the national or regional statistical data at a large spatial scale, a bias correction was performed on the Mouillot data. We calculated the ratio of burned area by the Mouillot data to GFED3.1 for 1997–2009 for each region (Fig. 2b) and also the globe. This ratio was then applied to correct for each decade the burned area data in the Mouillot dataset.

Note that the regional breakdowns of the globe by GFED3.1, and Mouillot and Field (2005) are different (Fig. 2). For comparison of burned area for the 20th century, the regional breakdown by Mouillot and Field (2005) was adopted as it is based on maximum temporal stability (error consistency), a highly important factor when comparing long-term data.

### 2.4.2 Fire patch data

Alaskan and Canadian fire management agencies have maintained historical fire monitoring for a relatively long time (dating back to 1950s). Their observations provide robust datasets for model validation of fire trend and variability. The historical fire information for the US state of Alaska was retrieved from the Alaska Interagency Coordination Center (AICC, [http://afsmaps.blm.gov/imf\\_firehistory/imf.jsp?site=firehistory](http://afsmaps.blm.gov/imf_firehistory/imf.jsp?site=firehistory)). The fire information for Canada was from the Canadian Wildland Fire Information System (<http://cwfis.cfs.nrcan.gc.ca/ha/nfdb>). These datasets contain information on fire location, fire size (burned area), fire date and fire cause. Note, in these two datasets fires *with all sizes* are included.

## Modelling global burned area and fire regime

C. Yue et al.

Title Page

Abstract

Introduction

Conclusions

References

Tables

Figures



Back

Close

Full Screen / Esc

Printer-friendly Version

Interactive Discussion



Archibald et al. (2010) classified the MCD45A1 500 m MODIS fire burned area data into individual fire patches for the southern African region. This fire patch information includes location, patch size (with minimum fire size of 0.25 km<sup>2</sup>), and the start and end dates of burning. The fire patch data for boreal North America and southern Africa are used to evaluate the model simulated fire size distribution (Fig. 3).

### 2.4.3 Fire season length, the 95th quantile fire size and 95th quantile fire intensity

Global observation datasets for fire season length, the 95th quantile fire size and 95th quantile fire intensity are provided by Archibald et al. (2013). The fire season length was quantified as the number of months required to reach 80 % of the total average annual burned area by using GFED3.1 data. The MCD45A1 burned area product at 500 m resolution was used to derive the individual fires by applying a flood-fill algorithm, and the 95th quantile fire size in each grid cell was extracted to represent the size of large fires. The fire intensity is approximated by fire radiative power (FRP), which is derived from the satellite middle-IR wavelength measurements sensed over actively burning fires. The MCD14ML active fire product was used to calculate the 95th quantile FRP as a proxy for the fireline intensity of large fires.

The fire season length simulated by the model was also quantified as the number of months required to reach 80 % of the simulated mean annual burned area for the period of 1997–2009. As a homogeneous set of fires with a single fire size is simulated by the model over a given grid cell on a daily time step, there is no corresponding fire patch information available on each grid cell. Thus the simulated daily mean fire size and fireline intensity over a given grid cell during the period of 1997–2009 were pooled together to create a “pool of fire patch”, which was further used to extract the 95th quantile of fire size and fireline intensity.

## Modelling global burned area and fire regime

C. Yue et al.

Title Page

Abstract

Introduction

Conclusions

References

Tables

Figures

◀

▶

◀

▶

Back

Close

Full Screen / Esc

Printer-friendly Version

Interactive Discussion



## 2.5 Metrics used to evaluate modelled burned area against GFED3.1 data

As the GFED3.1 data are most widely used by the fire modelling community, the model results are evaluated against GFED3.1 data for the period of 1997–2009. Three aspects were examined: the mean annual value of burned area, the similarity in interannual variability and the seasonality. The evaluation has been done for each GFED3.1 region (Fig. 2a).

For the model error in terms of mean annual burned area (BA), we use the relative difference:

$$E_{BA} = \frac{BA_{\text{model}} - BA_{\text{GFED}}}{BA_{\text{GFED}}} \quad (2)$$

where  $BA_{\text{model}}$  is the simulated burned area averaged over 1997–2009, and  $BA_{\text{GFED}}$  is GFED3.1 mean annual burned area for the same period. The similarity in interannual variability ( $S_{\text{interannual}}$ ) is estimated by the correlation coefficient of the two linearly detrended monthly burned area time series by model simulation and GFED3.1 data. Finally, the seasonality similarity ( $S_{\text{season}}$ ) is given by:

$$S_{\text{season}} = \sum_{i=1}^{12} \min(\text{frac\_model}_i, \text{frac\_GFED}_i) \quad (3)$$

where  $\text{frac\_model}_i$  and  $\text{frac\_GFED}_i$  are the fraction of burned area for the  $i$ th month relative to the annual burned area.

## 3 Results

### 3.1 Comparison of model simulation to satellite observation for the spatial and temporal pattern of burning

Figure 4 shows the spatial distribution of mean annual fire burned fraction for the model simulation result and for the three satellite-derived datasets (GFED3.1,

GLOBCARBON, L3JRC) for the period of 2001–2006. L3JRC and GLOBCARBON data show similar spatial patterns of burning, which is different from the GFED3.1 data. Generally, L3JRC and GLOBCARBON have less burned area in the Southern Hemisphere than GFED3.1 (see also Fig. 5), with smaller spatial extent of burning in the (wooded) grassland systems in Africa and Australia. By contrast, in the middle to high latitudes of the Northern Hemisphere, L3JRC and GLOBCARBON have more burned area than GFED3.1. All three datasets capture the grassland burning in central and eastern Asia.

ORCHIDEE coupled with SPITFIRE is generally able to reproduce the spatial distribution and magnitude of satellite-observed burned fraction. The simulated mean annual global burned area for 2001–2006 is  $329 \text{ Mha yr}^{-1}$ , which falls within the range of  $287\text{--}384 \text{ Mha yr}^{-1}$  given by the satellite observation data, and close to the  $344 \text{ Mha yr}^{-1}$  by the GFED3.1 dataset when crop fires are excluded.

Fires in grassland-dominated systems are well captured by the model, including steppe fires in central and east Asia, savanna fires in northern Africa, northern Australia and central to east South America. Two regions could be identified where model simulation is different from all the three observation datasets. One is the woodland savanna (miombo) in southern Africa, where burned area is underestimated by the model (simulated annual burned fraction is  $\sim 4\%$ , but  $14\text{--}24\%$  is observed). The other is western and central continental US (dominated by C3 and C4 grass in the land-cover map used by ORCHIDEE) where fires are overestimated by the model (simulated annual fraction is  $\sim 6\%$ , but  $1\text{--}2\%$  is observed). For the fires in high-latitude ( $> 45^\circ \text{ N}$ ) boreal forest and tundra, the magnitude of burned fraction by ORCHIDEE falls between that found in the GFED3.1 and in the L3JRC/GLOBCARBON datasets (Fig. 5).

The simulation pixels are divided into five classes according to their simulation quality, as shown in Fig. 4e. Table 1 shows the mean burned area for each category and dataset. The grid cells with burning collocated for both the model and observation data (labelled as ORC-good, ORC-max, ORC-min in Fig. 4) cover the majority of the global burned area (78% to 92% depending on different datasets), indicating that the model

## Modelling global burned area and fire regime

C. Yue et al.

Title Page

Abstract

Introduction

Conclusions

References

Tables

Figures

⏪

⏩

◀

▶

Back

Close

Full Screen / Esc

Printer-friendly Version

Interactive Discussion



can reproduce the major spatial extent of burning. However, discrepancy still remains, in that 50 % of the modelled burned area is classified as ORC-max (i.e., overestimation of burned fraction by the model), whereas observation datasets have half of the burned area labelled as ORC-min (i.e., underestimation of burned fraction by the model). Shifting from the single value of  $a(\text{ND})$  (0.22 over the globe in Eq. 1) to a spatial dataset did not improve the result (Supplement Table S1).

Figure 5 also illustrates the lower burned area found in L3JRC and GLOBCARBON in comparison with GFED3.1 for the Southern Hemisphere and subtropical Northern Hemisphere, in contrast to the higher burned area in the middle-to-high latitude region in the Northern Hemisphere. The simulated latitudinal distribution of burned area generally falls within the minimum-maximum range of the three observation products. Exceptions are the regions of  $\sim 5\text{--}15^\circ\text{S}$  and  $30\text{--}40^\circ\text{N}$ , corresponding to the underestimated burning in southern African savanna and the overestimate in western and central US, discussed above.

The interannual (12-months smoothed global total burned area) time series of burned area by the GFED3.1, model simulation and the GLOBCARBON data are quite similar, but the J3JRC data has a different temporal phase (Fig. 6). The model result agrees best with the GFED3.1 variability, except that the model fails to reproduce the 1998 peak burning. Shifting from the single  $a(\text{ND})$  value (0.22 over the globe) to the spatial dataset (Supplement Fig. S1) improves the agreement of the simulated global total burned area with the GFED3.1 data. This indicates that the model is able to reproduce the temporal trend of burning on the global scale as observed by the satellite data.

### 3.2 Model evaluation against GFED3.1 burned area data

The simulated burned area for 1997–2009 is evaluated against the GFED3.1 data for each region (shown in Fig. 2a) in terms of mean annual burned area, and similarity in the interannual variability and seasonality (see metrics in Sect. 2.5). The results are

## Modelling global burned area and fire regime

C. Yue et al.

Title Page

Abstract

Introduction

Conclusions

References

Tables

Figures



Back

Close

Full Screen / Esc

Printer-friendly Version

Interactive Discussion



presented in Table 2. The comparison of annual burned area at regional scale is shown in the Supplement Fig. S4.

The model error for the annual burned area (BA) is highest for the region of Middle East (MIDE, by a factor of 38, occupying 0.1 % vs. 2.9 % of global BA by GFED3.1 vs. ORCHIDEE) and lowest for the region of Boreal Asia (BOAS, by a factor of 0.1, occupying 1.6 % of global BA by both data). The model underestimates the burned area in the three biggest fire regions of the globe (Northern Hemisphere Africa, Southern Hemisphere Africa and Australia, together occupying 86 % vs. 45 % of global BA) by on average 53 %. Prominent model overestimation is found in Central Asia (CEAS, by a factor of 3.7, occupying 3 % vs. 15.8 % of global BA), and Southern Hemisphere South America (SHSA, by a factor of 1.6, occupying 5.5 % vs. 15.7 % of global BA).

The correlation coefficient for the linearly detrended global total annual burned area between the ORCHIDEE simulation and GFED3.1 is 0.57, indicating that the model captures the interannual variability of burned area rather well, because errors are compensated among regions. On regional scale, the similarity of interannual variability and seasonality between the model and GFED3.1 is generally good, with  $S_{\text{interannual}}$  values bigger than 0.5 and  $S_{\text{season}}$  bigger than 0.6 for most of the regions (Table 2).

### 3.3 Fire and precipitation relationship

The model captures well the empirical relationship between burned area and precipitation found in tropical and subtropical regions (Fig. 7; see also Prentice et al., 2011; van der Werf et al., 2008b). In low precipitation regions ( $< 400 \text{ mm yr}^{-1}$ ), the climate is favourable for fire but burning is limited by the available fuel. In contrast, regions with higher precipitation ( $> 2000 \text{ mm yr}^{-1}$ ) always support a relatively large fuel amount but fires are limited by the duration of the dry season when fires can occur. Burned area is maximal for regions with intermediate precipitation and productivity (Krawchuk and Moritz, 2010).

Maximum burning occurs around an annual precipitation of 1000 mm according to the model simulation, compared to 1200 mm by GFED3.1, and 1400 mm by the

## Modelling global burned area and fire regime

C. Yue et al.

Title Page

Abstract

Introduction

Conclusions

References

Tables

Figures



Back

Close

Full Screen / Esc

Printer-friendly Version

Interactive Discussion



GLOBCARBON and L3JRC datasets. GLOBCARBON and L3JRC show the lowest burning in this tropical/subtropical belt, followed by the model simulation, with the burned area by GFED3.1 being the highest. The fire and precipitation relationship was further divided into four sub-regions of America, Africa, Asia and Australia following van der Werf et al. (2008b) and the results are shown in Supplement Fig. S5. The model-observation agreement in fire-precipitation pattern is moderate in Africa and Australia, but low-precipitation fires are overestimated by the model in America and Asia.

### 3.4 Peak fire month and fire season length

The spatial distributions of the peak months for burned area by model simulation and as given by GFED3.1 are compared in Fig. 8. The peak fire month is defined as the month of the year with the maximum monthly burned area. The global spatial pattern of simulated peak fire month is in general agreement with that given by GFED3.1 data. The difference between simulated and observed peak month is quantified by the following index, after Prentice et al. (2011):

$$D_2 = \left[ 1 - \left( \frac{\sum_{j=1,n} A_j \cos \theta_j}{\sum_{j=1,n} A_j} \right) \right] / 2 \quad (4)$$

where  $\theta_j$  is the angle between vectors representing the simulated and observed peak fire month (with January to December resembling one to twelve on a clock),  $n$  is the total number of grid cells and  $A_j$  is the burned area by GFED3.1 data. According to Eq. (4), the value of  $D_2$  is zero when simulated peak month is perfectly in phase with the observation, 0.5 if the timing is off by 3 months in either direction, and one (the maximum) if the timing is off by 6 months. The model simulation gives  $D_2 = 0.51$ , indicating that the simulated and observed peak fire month differ by an average of three months. At regional scale, the simulated peak fire months for most regions are within one month of those given by the GFED3.1 data, with the exceptions of the Middle East and Southern Hemisphere Africa (see the far right hand column of Table 2). Refer to Supplement

## GMDD

7, 2377–2427, 2014

### Modelling global burned area and fire regime

C. Yue et al.

Title Page

Abstract

Introduction

Conclusions

References

Tables

Figures

◀

▶

◀

▶

Back

Close

Full Screen / Esc

Printer-friendly Version

Interactive Discussion



Fig. S6 for more details of the comparison of modelled and observed seasonal pattern of burning for different GFED3.1 regions.

Figure 9 compares the model results with the GFED3.1-derived fire season length from Archibald et al. (2013). The spatial pattern of the fire season length by model simulation agrees well with that given by Archibald et al. (2013), with the fire season length lasting 1–3 months in the boreal region, and 4–7 months in semi-arid grasslands and savannas. The fire season length in the southern fringe of northern African savanna, and in the savannas of southern Africa and South America seems to be underestimated by the model by 2–4 months.

### 3.5 Long-term trends of burned area during the 20th century

Over the 20th century, the historical trend of modelled global total burned area generally follows the Mouillot reconstruction data (Mouillot and Field, 2005) as corrected by GFED3.1 data (see Sect. 2.4.1), with a gradually increasing burned area after the 1930s until the 1990s, after which global burned area began to decrease (Fig. 10). Regionally, simulated trends in burned area agree best with the Mouillot data in boreal Russia. The simulated burned area also agrees well with fire agency survey data for the US state of Alaska and Canada (Supplement Fig. S7). This reflects the model capability to capture fire trends driven by climate variation relatively well. This agreement also suggests that the CRU-NCEP climate data can be used for simulating trends in fires despite the uncertainties. The model fails, however, to capture burned area trends for regions where fires resulting from changed land use likely played a bigger role in the earlier 20th century according to Mouillot data (Mouillot and Field, 2005), e.g., Australia and New Zealand, USA and southern South America, or in regions where the implementation of modern fire prevention has drastically reduced the burned area, as occurred in the 1960s in boreal North America.

## Modelling global burned area and fire regime

C. Yue et al.

Title Page

Abstract

Introduction

Conclusions

References

Tables

Figures

◀

▶

◀

▶

Back

Close

Full Screen / Esc

Printer-friendly Version

Interactive Discussion



### 3.6 Fire size distribution in boreal North America and southern Africa

Above a certain threshold, the relationship between the number of fires and fire patch size conforms to the power-law distribution (Malamud et al., 1998, 2005) and can be described as:

$$N = \alpha \times S^{-\beta} \quad (5)$$

where  $N$  is the number of fires,  $S$  is the individual fire patch size,  $\beta$  is the slope on a log-log plot. In this section we compare the simulated fire size distribution against observational data over two regions: boreal North America and southern Africa (see map in Fig. 3).

The simulated daily fire number and mean fire size for the same period as the observation data were used to generate the modelled fire patch data. For both simulated and observed fires, all fires within the test region were pooled together. Fires were binned according to the fire size in an equal logarithmic distance manner (with the minimum–maximum size range being divided into 100 bins). The mean annual number of fires on an area basis for each bin was calculated.

The minimum fire size for southern Africa given by Archibald et al. (2010) is 25 ha (which is the resolution of a 500 m MODIS burned area pixel) and this value was arbitrarily used as the fire size threshold in the regression analysis for both regions. The mean value of each size range is used as the explaining variable. Both fire number and fire size data are log transformed, and OLS regression is used to estimate the parameter values (slope beta, intercept alpha).

For both boreal North America and the southern Africa, the slopes obtained from the model simulation are higher than the ones derived from fire management agency data (boreal North America) or satellite-derived data (southern Africa) (Fig. 11). This indicates that the simulated fire distribution is skewed towards small fires and that the number of big fires is underestimated. However, the model successfully reproduced the power-law (heavy-tailed) distribution pattern of fires.

## Modelling global burned area and fire regime

C. Yue et al.

Title Page

Abstract

Introduction

Conclusions

References

Tables

Figures

⏪

⏩

◀

▶

Back

Close

Full Screen / Esc

Printer-friendly Version

Interactive Discussion



We further calculate the cumulative fraction of the total burned area by fires below a given quantile of fire size (the minimum size, every tenth quantile from 10th to 90th quantile, and the maximum size) (Fig. 12). According to the observation data, in boreal North America, the total burned area is mainly dominated by a few big fires, with the top 10 % of fires (90th quantile to the maximum size) accounting for 99.8 % of the total burned area. By contrast, the same group of fires (i.e., the highest 10 % big fires) account for only ~ 60 % of the simulated total burned area, with the remaining being accounted for by many small fires. For southern Africa, the satellite observation data show the top 30 % of fires (70th quantile to the maximum size) make up 90 % of the total burned area, whereas the model simulates 90 % of the total burned area coming from half of all fires (median to the maximum size).

### 3.7 Model evaluation for the 95th quantile fire size and 95th quantile fire intensity

Figure 13 compares the simulated 95th quantile fire size with the global observations. According to the observation data, the biggest fires (500–10 000 km<sup>2</sup>) are grassland-dominated fires in central and eastern Asia, African savanna and northern Australia, followed by fires (50–500 km<sup>2</sup>) in the Russian and Alaskan boreal forest, and woodland fires in Africa. Fires in the in the rest of the world are relatively small (< 50 km<sup>2</sup>). In terms of spatial pattern of fire size distribution, the model could reproduce the biggest fires in grassland-dominated systems in central and eastern Asia, northern Australia and part of the tundra fires (10–250 km<sup>-2</sup>), as well as the big fires in Alaska and northern Canada (50–500 km<sup>2</sup>), but the fire sizes for vast regions of African and south American savanna and woodland savanna are quite small (< 10 km<sup>2</sup>).

The FRP quantifies the energy released per unit of time by an active fire based on the pixel area of the satellite, while the fireline intensity is the rate of heat transfer per unit length of the fireline (kW m<sup>-1</sup>) (Byram 1959). Thus the FRP can only function as a temporally and spatially continuous proxy for the fireline intensity over the globe, as the length of flame front is needed to convert the former into the latter (Archibald



level, with model underestimation mainly in the savanna of Africa and Australia, and overestimation mainly in central Asia and Southern Hemisphere South America.

The model can reproduce the maximal burned area for the intermediate range of annual precipitation for the tropical and subtropical regions (35° S–35° N) (also shown by Prentice et al., 2011; van der Werf et al., 2008b), indicating that precipitation, as an important driver for fire, has been successfully captured by the model. For the boreal region where climate plays a dominant role in determining the long-term trend of burned area, the simulated burned area generally agrees well with the historical reconstruction data (boreal Russia for 1920–2009) and the government fire agency data (US state of Alaska and Canada for 1950–2009), indicating that the model is capturing the climate as a driver of fire. However, on the global scale because the fire trend is determined by multiple factors including climate, land-use practice and fire suppression (Mouillot and Field, 2005), the simulated burned area trend only agrees moderately well with the reconstruction data for the 20th century.

## 4.2 Potential sources of systematic errors

Fire is a complex, regional process that involves dimensions of vegetation, climate and human activity (Bowman et al., 2009). The uncertainties in all these factors will contribute to the overall uncertainty in simulated fire activities. Because SPITFIRE simulates fire occurrence through a complex chain that includes multiple processes from potential ignition to fire climate, to fire spread rate and tree mortality, identifying the contributions of each modelling step to the ultimate error in the simulated fire regime is problematic. A complete error analysis involving all the model parameters is beyond the scope of this study, but the following sections are intended to serve as preliminary investigation of model errors.

## Modelling global burned area and fire regime

C. Yue et al.

Title Page

Abstract

Introduction

Conclusions

References

Tables

Figures

◀

▶

◀

▶

Back

Close

Full Screen / Esc

Printer-friendly Version

Interactive Discussion



## 4.2.1 Ignition sources and fire numbers

On the global scale, due to the limitation of fire by fuel load on the dry regions, the modelled annual burned area is more closely related to the total fire numbers rather than the fire danger index (Supplement Fig. S8). This might lead to speculation that the potential ignition source is the first identified source of error for the simulated burned area. However, the shift from a constant uniform value of  $a(\text{ND}) = 0.22$  in the human ignition equation to the spatial dataset (Supplement Fig. S1) does not significantly improve the regional model-observation agreement (Supplement Fig. S2). The other possible error in ignition is that potential lightning ignitions are not suppressed by humans in densely populated areas, which might cause lightning-ignited fires being overestimated. We have tested this possibility by applying a population density dependent human suppression of lightning-ignited fires following Li et al. (2012), and the result showed that part of the overestimation of burned fraction in western US and central South America could be reduced (Fig. 4 and Supplement Fig. S9), but the burned area in Africa was further underestimated.

Published fire models (Kloster et al., 2012; Li et al., 2012; Pechony and Shindell, 2009; Venevsky et al., 2002) generally include ignitions from both lightning and human sources, together with explicit or implicit human suppression of fires. However, one common challenge is to properly calibrate ignition parameters. One option is to use active fire counts (as in case of Li et al., 2012; Pechony and Shindell, 2009), but fire counts are not exactly real fire numbers, because a single widespread fire could be seen as many fire counts and the burned area per hotspot could vary by an order of magnitude depending on vegetation composition (Hantson et al., 2013). Little information is provided in the literature on the comparison of simulated and observed fire numbers.

We compared the simulated number of fires with the observed fire patch number for Canada and southern Africa (Supplement Fig. S10). Simulated fire numbers are higher than observation in both regions, with an overestimation of  $\sim 70\%$  in Canada and

GMDD

7, 2377–2427, 2014

### Modelling global burned area and fire regime

C. Yue et al.

Title Page

Abstract

Introduction

Conclusions

References

Tables

Figures



Back

Close

Full Screen / Esc

Printer-friendly Version

Interactive Discussion



~ 140 % in southern Africa. However it should be noted that the observation data are also subject to error, as very small fires might be missed in the Canadian fire agency survey data. The fire patch data given by Archibald et al. (2010) were reclassified from MODIS 500 m burned area data and as a result the fires smaller than 0.25 km<sup>2</sup> threshold will be missed. To make the model practically useful for burned area prediction at the regional scale, in principle one could use the ratio of observed to the simulated burned area to correct the potential ignition numbers when there is a lack of observed fire patch data (ideally separated by different sources).

#### 4.2.2 Fire size

Our simulated burned area for Canada agrees well with the fire agency survey data (Supplement Fig. S7), but simulated burned area for southern Africa is 60 % lower than GFED3.1 data (Table 2). Given the overestimation of the number of fires, the mean fire size is underestimated by the model. The fire size distribution analysis reveals that the model mainly underestimates the number and size of the large fires in these two regions. Over the globe, despite the fact that the model correctly identifies some of the regions where large fires occur (mainly with grassland fraction higher than ~ 70 % by the land cover used in the model), the large fire size is grossly underestimated in the model – by up to two orders of magnitude (Fig. 13).

Within the model, the fire size is determined by the fire duration time and fire spread rate. Fire spread rate is determined using the Rothermel equation (Rothermel, 1972; Wilson, 1982) and depends on multiple factors including wind speed, fuel bulk density, net fuel load and fuel packing ratio, etc. To gain some insight into the model's behaviour, we tried to relate the 95th quantile fire size to some parameters (grassland fraction, fuel bulk density). As shown in Supplement Fig. S11, the size of large fires is exponentially dependent on the fire spread rate. The fire spread rate is very sensitive to the fuel bulk density and grass fraction beyond some threshold (e.g., fire spread rate surges when grass coverage exceeds ~ 70 %), with the fuel bulk density being inversely dependent on the grass fraction. Thus the simulated fire size could be sensitive to the land-cover

## Modelling global burned area and fire regime

C. Yue et al.

Title Page

Abstract

Introduction

Conclusions

References

Tables

Figures



Back

Close

Full Screen / Esc

Printer-friendly Version

Interactive Discussion





a 0.5° grid cell, the model simulates (on a daily basis and when fire does occur on a specific day) a given number of homogeneous fires with a single fire size, while in reality a big fire might grow from a single or multiple ignitions (in the case of separate fires merging with each other) over a period of days or even weeks (Keeley et al., 2009).

The daily time step of the model does not allow fires to span more than one day.

To fully represent the big fire process in reality, improvements need to be made to the model to allow fire to span multiple days when the climate is favourable. More mechanistic process modelling is needed, for example, by incorporating the information on fuel, weather and topography to predict the fire extinction.

#### 4.2.5 Influence of fire-climate-vegetation feedback

In the current simulation the dynamic vegetation module of ORCHIDEE was switched off and a static land-cover map was used. Tree mortality was affected by fire-induced tree damage, but tree coverage within a given grid cell was static and not allowed to vary with fire occurrence. A test simulation has been done for Southern Hemisphere Africa following the same simulation protocol as in Sect. 2.3 but with the dynamic vegetation module being switched on, in order to investigate the simulated fire behaviour with dynamic vegetation. Supplement Fig. S13 compares the simulated annual burned area, grass and tree coverage change and the fire danger index for 1901–2009 with the model in dynamic and static vegetation modes.

In dynamic vegetation mode, the simulated burned area suddenly begins to increase around 1965, in response to increased fire danger index. The increase in fire activity further increases the grass coverage and reduces tree coverage, causing a positive feedback to finally induce a peak of burned area around 1975, after which the burned area decreases. In static vegetation mode, the simulated burned area shows a similar peak in response to the peak in the fire danger index, however, with a much smaller peak of burned area than that simulated in dynamic vegetation mode because of the lack of fire-vegetation-climate feedback. The simulated burned area by both simulations is still lower than that given by the GFED3.1 data for the period of 1997–2009, although

## Modelling global burned area and fire regime

C. Yue et al.

Title Page

Abstract

Introduction

Conclusions

References

Tables

Figures

◀

▶

◀

▶

Back

Close

Full Screen / Esc

Printer-friendly Version

Interactive Discussion



the peak burned area in the dynamic vegetation mode is comparable with GFED3.1 data.

This test indicates that including the fire-climate-vegetation feedback could improve the simulation when the climate is favourable for fire occurrence. At the same time, it also suggests that other factors like climate, and the model mechanisms determining the competitiveness of trees vs. grass might also play a role in the error of fire modelling.

#### 4.2.6 Summary

The preliminary investigation of modelling error reveals that fire size is generally underestimated by the model over the entire globe and the ignition error is playing an important role in determining the ultimate simulated burned area. On the regional scale, ignition numbers (fire numbers) are either overestimated to compensate the fire size underestimation to cause a moderate or overestimated burned area, or are not enough that the simulated burned area is underestimated as well. The underestimation of fire size is most likely due to the constrained maximum fire duration time, although in some regions the fire spread rate is also underestimated relative to measured data.

#### 4.3 Future model improvement directions and needed datasets

Currently many efforts in global fire modelling are directed at reproducing the temporal and spatial pattern of burned areas (Kloster et al., 2010; Li et al., 2012; Prentice et al., 2011; Thonicke et al., 2010). Total burned area is determined by ignition frequency and fire size, which itself is controlled by fire spread rate (fire intensity) and fire duration. More work is needed to investigate if a model can reproduce the mechanisms that drive burned area: i.e. the rate of spread, fire duration, fire size, ignition frequency, and fireline intensity. Comparing observed and simulated fire regimes, which combine information on fire timing (fire season), size, numbers and intensity (Gill and Allan,

## GMDD

7, 2377–2427, 2014

### Modelling global burned area and fire regime

C. Yue et al.

Title Page

Abstract

Introduction

Conclusions

References

Tables

Figures

◀

▶

◀

▶

Back

Close

Full Screen / Esc

Printer-friendly Version

Interactive Discussion



2008) will help to reveal gaps in this understanding. The present study is a step in this direction, bringing new in-depth model evaluation.

In summary, the fire processes in the SPITFIRE model are complex enough to include many aspects of wildland and human-caused fire processes in nature. However, little is known about the parameter sensitivities and their contribution to model error. The simulated intermediate model parameters (e.g., fire numbers, fire size, fire spread rate, fire intensity) are poorly constrained by the observation data. As a result, error compensation could be prevalent in the model and a wider application of the model is impeded.

To advance model development, global measurement datasets of the key fire parameters, including fire spread rate, fuel bulk density, wind speed, fire intensity, fire duration, etc., should be established and used to calibrate fire models. On the other hand, the complexity of fire model parameters and the regional nature of fire processes make it unlikely that these parameters could be calibrated in a parameter-by-parameter and site-by-site way, but some more advanced techniques such as data assimilation or model-data fusion could be helpful.

Finally, we should consider incorporating some more mechanistic fire processes into the model, such as crown fire spread, impacts of land fragmentation, multi-day fire duration, topography effects, and the mechanistic process of fire extinction.

## 5 Conclusions

We have integrated the SPITFIRE model into a global process-based vegetation model ORCHIDEE. The historical burned area for the 20th century was simulated and the modelled fire regime was evaluated against observation data. The model was able to capture well the historical climatic drivers of the burned area for the 20th century. However, parameter uncertainties such as number of fire ignitions and fire spread rate result in considerable regional discrepancies. Fire sizes are generally underestimated, with the error in simulated burned area being partly compensated by overestimated fire

# GMDD

7, 2377–2427, 2014

## Modelling global burned area and fire regime

C. Yue et al.

Title Page

Abstract

Introduction

Conclusions

References

Tables

Figures

⏪

⏩

◀

▶

Back

Close

Full Screen / Esc

Printer-friendly Version

Interactive Discussion



numbers. Future model development requires a complete parameter sensitivity analysis for the key processes represented in fire modeling. To constrain the model error, consistent spatial observational datasets should be established for validating the key variables in the model at different modelling steps.

5 **Supplementary material related to this article is available online at <http://www.geosci-model-dev-discuss.net/7/2377/2014/gmdd-7-2377-2014-supplement.pdf>.**

*Acknowledgements.* This study was supported by the fire\_cci project (<http://www.esa-fire-cci.org/>), funded by the European Space Agency. The authors would like to thank Nicolas Vuichard, Arnaud Caubel, and Josefine Ghattas for their kind technical help.

## References

- Archibald, S., Scholes, R. J., Roy, D. P., Roberts, G., and Boschetti, L.: Southern African fire regimes as revealed by remote sensing, *Int. J. Wildland Fire*, 19, 861–878, 2010.
- Archibald, S., Lehmann, C. E. R., Gómez-Dans, J. L., and Bradstock, R. A.: Defining pyromes and global syndromes of fire regimes, *P. Natl. Acad. Sci. USA*, 110, 6442–6447, doi:10.1073/pnas.1211466110, 2013.
- Arora, V. K. and Boer, G. J.: Fire as an interactive component of dynamic vegetation models, *J. Geophys. Res.-Biogeo.*, 110, G02008, doi:10.1029/2005JG000042, 2005.
- Barrett, K., McGuire, A. D., Hoy, E. E., and Kasischke, E. S.: Potential shifts in dominant forest cover in interior Alaska driven by variations in fire severity, *Ecol. Appl.*, 21, 2380–2396, doi:10.1890/10-0896.1, 2011.
- Beck, P. S. A., Goetz, S. J., Mack, M. C., Alexander, H. D., Jin, Y., Randerson, J. T., and Lorrant, M. M.: The impacts and implications of an intensifying fire regime on Alaskan boreal forest composition and albedo, *Glob. Change Biol.*, 17, 2853–2866, doi:10.1111/j.1365-2486.2011.02412.x, 2011.
- Bond, W. J., Woodward, F. I., and Midgley, G. F.: The global distribution of ecosystems in a world without fire, *New Phytol.*, 165, 525–537, doi:10.1111/j.1469-8137.2004.01252.x, 2005.
- Bowman, D. M. J. S., Balch, J. K., Artaxo, P., Bond, W. J., Carlson, J. M., Cochrane, M. A., D'Antonio, C. M., DeFries, R. S., Doyle, J. C., Harrison, S. P., Johnston, F. H., Keeley, J. E.,

## Modelling global burned area and fire regime

C. Yue et al.

Title Page

Abstract

Introduction

Conclusions

References

Tables

Figures

◀

▶

◀

▶

Back

Close

Full Screen / Esc

Printer-friendly Version

Interactive Discussion



## Modelling global burned area and fire regime

C. Yue et al.

Title Page

Abstract

Introduction

Conclusions

References

Tables

Figures

⏪

⏩

◀

▶

Back

Close

Full Screen / Esc

Printer-friendly Version

Interactive Discussion



Krawchuk, M. A., Kull, C. A., Marston, J. B., Moritz, M. A., Prentice, I. C., Roos, C. I., Scott, A. C., Swetnam, T. W., van der Werf, G. R., and Pyne, S. J.: Fire in the Earth System, *Science*, 324, 481–484, doi:10.1126/science.1163886, 2009.

Burton, P. J., Parisien, M., Hicke, J. A., Hall, R. J., and Freeburn, J. T.: Large fires as agents of ecological diversity in the North American boreal forest, *Int. J. Wildland Fire*, 17, 754–767, 2008.

Byram, G. M.: Combustion of forest fuels, in: *Forest Fire: Control and Use*, 1st edn., edited by: Davis, K. P., McGraw-Hill Book Company, New York, 61–89, 1959.

Cecil, D. J., Buechler, D. E., and Blakeslee, R. J.: Gridded lightning climatology from TRMM-LIS and OTD: dataset description, *Atmos. Res.*, doi:10.1016/j.atmosres.2012.06.028, 2012.

Daniau, A.-L., Goñi, M. F. S., Martinez, P., Urrego, D. H., Bout-Roumazeilles, V., Desprat, S., and Marlon, J. R.: Orbital-scale climate forcing of grassland burning in southern Africa, *P. Natl. Acad. Sci. USA*, 110, 5069–5073, doi:10.1073/pnas.1214292110, 2013.

Giglio, L., Randerson, J. T., van der Werf, G. R., Kasibhatla, P. S., Collatz, G. J., Morton, D. C., and DeFries, R. S.: Assessing variability and long-term trends in burned area by merging multiple satellite fire products, *Biogeosciences*, 7, 1171–1186, doi:10.5194/bg-7-1171-2010, 2010.

Gill, A. M. and Allan, G.: Large fires, fire effects and the fire-regime concept, *Int. J. Wildland Fire*, 17, 688–695, 2008.

Hantson, S., Padilla, M., Corti, D., and Chuvieco, E.: Strengths and weaknesses of MODIS hotspots to characterize global fire occurrence, *Remote Sens. Environ.*, 131, 152–159, doi:10.1016/j.rse.2012.12.004, 2013.

Hoffmann, W. A., Geiger, E. L., Gotsch, S. G., Rossatto, D. R., Silva, L. C. R., Lau, O. L., Haridasan, M., and Franco, A. C.: Ecological thresholds at the savanna-forest boundary: how plant traits, resources and fire govern the distribution of tropical biomes, *Ecol. Lett.*, 15, 759–768, doi:10.1111/j.1461-0248.2012.01789.x, 2012.

Kasischke, E. S. and Hoy, E. E.: Controls on carbon consumption during Alaskan wildland fires, *Glob. Change Biol.*, 18, 685–699, doi:10.1111/j.1365-2486.2011.02573.x, 2012.

Kasischke, E. S. and Turetsky, M. R.: Recent changes in the fire regime across the North American boreal region – Spatial and temporal patterns of burning across Canada and Alaska, *Geophys. Res. Lett.*, 33, L09703, doi:10.1029/2006GL025677, 2006.

Kasischke, E. S., Verbyla, D. L., Rupp, T. S., McGuire, A. D., Murphy, K. A., Jandt, R., Barnes, J. L., Hoy, E. E., Duffy, P. A., Calef, M., and Turetsky, M. R.: Alaska's changing

## Modelling global burned area and fire regime

C. Yue et al.

Title Page

Abstract

Introduction

Conclusions

References

Tables

Figures

◀

▶

◀

▶

Back

Close

Full Screen / Esc

Printer-friendly Version

Interactive Discussion



fire regime – implications for the vulnerability of its boreal forests, *Can. J. For. Res.*, 40, 1313–1324, doi:10.1139/X10-098, 2010.

Keeley, J. E., Fotheringham, C. J., and Morais, M.: Reexamining Fire Suppression Impacts on Brushland Fire Regimes, *Science*, 284, 1829–1832, doi:10.1126/science.284.5421.1829, 1999.

Keeley, J. E., Safford, H., Fotheringham, C. J., Franklin, J., and Moritz, M.: The 2007 Southern California Wildfires: lessons in Complexity, *J. Forest.*, 107, 287–296, 2009.

Kloster, S., Mahowald, N. M., Randerson, J. T., Thornton, P. E., Hoffman, F. M., Levis, S., Lawrence, P. J., Feddema, J. J., Oleson, K. W., and Lawrence, D. M.: Fire dynamics during the 20th century simulated by the Community Land Model, *Biogeosciences*, 7, 1877–1902, doi:10.5194/bg-7-1877-2010, 2010.

Kloster, S., Mahowald, N. M., Randerson, J. T., and Lawrence, P. J.: The impacts of climate, land use, and demography on fires during the 21st century simulated by CLM-CN, *Biogeosciences*, 9, 509–525, doi:10.5194/bg-9-509-2012, 2012.

Krawchuk, M. A. and Moritz, M. A.: Constraints on global fire activity vary across a resource gradient, *Ecology*, 92, 121–132, doi:10.1890/09-1843.1, 2010.

Krinner, G., Viovy, N., de Noblet-Ducoudré, N., Ogée, J., Polcher, J., Friedlingstein, P., Ciais, P., Sitch, S., and Prentice, I. C.: A dynamic global vegetation model for studies of the coupled atmosphere-biosphere system, *Global Biogeochem. Cy.*, 19, GB1015, doi:10.1029/2003GB002199, 2005.

Langmann, B., Duncan, B., Textor, C., Trentmann, J., and van der Werf, G. R.: Vegetation fire emissions and their impact on air pollution and climate, *Atmos. Environ.*, 43, 107–116, doi:10.1016/j.atmosenv.2008.09.047, 2009.

Li, F., Zeng, X. D., and Levis, S.: A process-based fire parameterization of intermediate complexity in a Dynamic Global Vegetation Model, *Biogeosciences*, 9, 2761–2780, doi:10.5194/bg-9-2761-2012, 2012.

Magi, B. I., Rabin, S., Shevliakova, E., and Pacala, S.: Separating agricultural and non-agricultural fire seasonality at regional scales, *Biogeosciences*, 9, 3003–3012, doi:10.5194/bg-9-3003-2012, 2012.

Malamud, B. D., Morein, G., and Turcotte, D. L.: Forest fires: an example of self-organized critical behavior, *Science*, 281, 1840–1842, doi:10.1126/science.281.5384.1840, 1998.

## Modelling global burned area and fire regime

C. Yue et al.

[Title Page](#)
[Abstract](#)
[Introduction](#)
[Conclusions](#)
[References](#)
[Tables](#)
[Figures](#)
[Back](#)
[Close](#)
[Full Screen / Esc](#)
[Printer-friendly Version](#)
[Interactive Discussion](#)


Malamud, B. D., Millington, J. D. A., and Perry, G. L. W.: Characterizing wildfire regimes in the United States, *P. Natl. Acad. Sci. USA*, 102, 4694–4699, doi:10.1073/pnas.0500880102, 2005.

Marlier, M. E., DeFries, R. S., Voulgarakis, A., Kinney, P. L., Randerson, J. T., Shindell, D. T., Chen, Y., and Faluvegi, G.: El Nino and health risks from landscape fire emissions in south-east Asia, *Nature Clim. Change*, 3, 131–136, doi:10.1038/nclimate1658, 2013.

Mouillot, F. and Field, C. B.: Fire history and the global carbon budget: a 1 degrees × 1 degrees fire history reconstruction for the 20th century, *Glob. Change Biol.*, 11, 398–420, 2005.

Pausas, J. G. and Keeley, J. E.: A burning story: the role of fire in the history of life, *BioScience*, 59, 593–601, doi:10.1525/bio.2009.59.7.10, 2009.

Pechony, O. and Shindell, D. T.: Fire parameterization on a global scale, *J. Geophys. Res.-Atmos.*, 114, D16115, doi:10.1029/2009JD011927, 2009.

Peterson, D. L. and Ryan, K. C.: Modeling postfire conifer mortality for long-range planning, *Environ. Manage.*, 10, 797–808, doi:10.1007/BF01867732, 1986.

Plummer, S., Arino, O., Ranera, F., Tansey, K., Chen, J., Dedieu, G., Eva, H., Piccolini, I., Borstlap, G., Beusen, B., Fierens, F., Heyns, W., Benedetti, R., Lacaze, R., Garrigues, S., Quaife, T., De Kauwe, M., Quegan, S., Raupach, M., Briggs, P., Poulter, B., Bondeau, A., Rayner, P., Schultz, M., Gobron, N., and McCallum, I.: An update on the Globcarbon initiative: multi-sensor estimation of global biophysical products for global terrestrial carbon studies, [online] available at: <http://eprints.ucl.ac.uk/179082/> (last access: 30 June 2011), 2007.

Poulter, B., Ciais, P., Hodson, E., Lischke, H., Maignan, F., Plummer, S., and Zimmermann, N. E.: Plant functional type mapping for earth system models, *Geosci. Model Dev.*, 4, 993–1010, doi:10.5194/gmd-4-993-2011, 2011.

Prentice, I. C., Kelley, D. I., Foster, P. N., Friedlingstein, P., Harrison, S. P., and Bartlein, P. J.: Modeling fire and the terrestrial carbon balance, *Global Biogeochem. Cy.*, 25, GB3005, doi:201110.1029/2010GB003906, 2011.

Randerson, J. T., Liu, H., Flanner, M. G., Chambers, S. D., Jin, Y., Hess, P. G., Pfister, G., Mack, M. C., Treseder, K. K., Welp, L. R., Chapin, F. S., Harden, J. W., Goulden, M. L., Lyons, E., Neff, J. C., Schuur, E. a. G., and Zender, C. S.: The impact of boreal forest fire on climate warming, *Science*, 314, 1130–1132, doi:10.1126/science.1132075, 2006.

Rogers, B. M., Randerson, J. T., and Bonan, G. B.: High-latitude cooling associated with landscape changes from North American boreal forest fires, *Biogeosciences*, 10, 699–718, doi:10.5194/bg-10-699-2013, 2013.

## Modelling global burned area and fire regime

C. Yue et al.

Title Page

Abstract

Introduction

Conclusions

References

Tables

Figures

◀

▶

◀

▶

Back

Close

Full Screen / Esc

Printer-friendly Version

Interactive Discussion



Rothermel, R. C.: A mathematical model for predicting fire spread in wildland fuels, Res. Pap. INT-115, Ogden, UT: US Department of Agriculture, Intermountain Forest and Range Experiment Station, 40 pp., available at: [http://www.fs.fed.us/rm/pubs\\_int/int\\_rp115.pdf](http://www.fs.fed.us/rm/pubs_int/int_rp115.pdf) (last access: 7 April 2014), 1972.

5 Schoennagel, T., Smithwick, E. A. H., and Turner, M. G.: Landscape heterogeneity following large fires: insights from Yellowstone National Park, USA, *Int. J. Wildland Fire*, 17, 742–753, 2008.

Smith, A. M. S. and Wooster, M. J.: Remote classification of head and backfire types from MODIS fire radiative power and smoke plume observations, *Int. J. Wildland Fire*, 14, 249–254, 2005.

10 Stocks, B. J., Mason, J. A., Todd, J. B., Bosch, E. M., Wotton, B. M., Amiro, B. D., Flannigan, M. D., Hirsch, K. G., Logan, K. A., Martell, D. L., and Skinner, W. R.: Large forest fires in Canada, 1959–1997, *J. Geophys. Res.-Atmos.*, 107, 8149, doi:10.1029/2001JD000484, 2002.

15 Tansey, K., Grégoire, J.-M., Defourny, P., Leigh, R., Pekel, J.-F., van Bogaert, E., and Bartholomé, E.: A new, global, multi-annual (2000–2007) burnt area product at 1 km resolution, *Geophys. Res. Lett.*, 35, L01401, doi:10.1029/2007GL031567, 2008.

Thonicke, K., Venevsky, S., Sitch, S., and Cramer, W.: The role of fire disturbance for global vegetation dynamics: coupling fire into a Dynamic Global Vegetation Model, *Global. Ecol. Biogeogr.*, 10, 661–677, 2001.

20 Thonicke, K., Spessa, A., Prentice, I. C., Harrison, S. P., Dong, L., and Carmona-Moreno, C.: The influence of vegetation, fire spread and fire behaviour on biomass burning and trace gas emissions: results from a process-based model, *Biogeosciences*, 7, 1991–2011, doi:10.5194/bg-7-1991-2010, 2010.

25 Tosca, M. G., Randerson, J. T., and Zender, C. S.: Global impact of smoke aerosols from landscape fires on climate and the Hadley circulation, *Atmos. Chem. Phys.*, 13, 5227–5241, doi:10.5194/acp-13-5227-2013, 2013.

Turner, M. G., Hargrove, W. W., Gardner, R. H., and Romme, W. H.: Effects of fire on landscape heterogeneity in Yellowstone National Park, Wyoming, *J. Veg. Sci.*, 5, 731–742, doi:10.2307/3235886, 1994.

30 Van der Werf, G. R., Dempewolf, J., Trigg, S. N., Randerson, J. T., Kasibhatla, P. S., Giglio, L., Murdiyarso, D., Peters, W., Morton, D. C., Collatz, G. J., Dolman, A. J., and DeFries, R. S.:

## Modelling global burned area and fire regime

C. Yue et al.

Title Page

Abstract

Introduction

Conclusions

References

Tables

Figures

◀

▶

◀

▶

Back

Close

Full Screen / Esc

Printer-friendly Version

Interactive Discussion



Climate regulation of fire emissions and deforestation in equatorial Asia, *P. Natl. Acad. Sci. USA*, 105, 20350–20355, doi:10.1073/pnas.0803375105, 2008a.

Van der Werf, G. R., Randerson, J. T., Giglio, L., Gobron, N., and Dolman, A. J.: Climate controls on the variability of fires in the tropics and subtropics, *Global Biogeochem. Cy.*, 22, GB3028, doi:10.1029/2007GB003122, 2008b.

Van der Werf, G. R., Randerson, J. T., Giglio, L., Collatz, G. J., Mu, M., Kasibhatla, P. S., Morton, D. C., DeFries, R. S., Jin, Y., and van Leeuwen, T. T.: Global fire emissions and the contribution of deforestation, savanna, forest, agricultural, and peat fires (1997–2009), *Atmos. Chem. Phys.*, 10, 11707–11735, doi:10.5194/acp-10-11707-2010, 2010.

van Leeuwen, T. T., van der Werf, G. R., Hoffman, A. A., Detmers, R. G., Archibald, S., Cook, G. D., de Groot, W. J., French, N. H. F., Kasischke, E. S., Savadogo, P., McCarty, J. L., Alvarado, E. C., Boschetti, L., Carvalho Jr. J. A., Hély C., Kloster, S., Meyer, C. P., Pettinari, M. L., Rucker G., Siegert, F., Solichin, S., Trollope, L. A., and Trollope, W. S. W.: Biomass burning fuel consumption rates: a field measurement database, *Biogeosciences*, in preparation, 2014.

Venevsky, S., Thonicke, K., Sitch, S., and Cramer, W.: Simulating fire regimes in human-dominated ecosystems: Iberian Peninsula case study, *Glob. Change Biol.*, 8, 984–998, doi:10.1046/j.1365-2486.2002.00528.x, 2002.

Ward, D. S., Kloster, S., Mahowald, N. M., Rogers, B. M., Randerson, J. T., and Hess, P. G.: The changing radiative forcing of fires: global model estimates for past, present and future, *Atmos. Chem. Phys.*, 12, 10857–10886, doi:10.5194/acp-12-10857-2012, 2012.

Westerling, A. L., Hidalgo, H. G., Cayan, D. R., and Swetnam, T. W.: Warming and earlier spring increase western US forest wildfire activity, *Science*, 313, 940–943, 2006.

Westerling, A. L., Turner, M. G., Smithwick, E. A. H., Romme, W. H., and Ryan, M. G.: Continued warming could transform Greater Yellowstone fire regimes by mid-21st century, *P. Natl. Acad. Sci. USA*, 108, 13165–13170, doi:10.1073/pnas.1110199108, 2011.

Wilson, R. A. J.: A reexamination of fire spread in free-burning porous fuel beds [Wildland fuels, forest fire management, model], USDA Forest Service Research Paper INT (USA) [online], available at: <http://agris.fao.org/agris-search/search.do?f=1983/US/US83048.xml;US8236661> (last access: 15 February 2014), 1982.

## Modelling global burned area and fire regime

C. Yue et al.

Title Page

Abstract

Introduction

Conclusions

References

Tables

Figures

◀

▶

◀

▶

Back

Close

Full Screen / Esc

Printer-friendly Version

Interactive Discussion



**Table 1.** Mean annual burned area ( $\text{Mha yr}^{-1}$ ) for the period of 2001–2006 for different ORCHIDEE simulation quality as shown in Fig. 4.

	ORCHIDEE	GFED3.1	GLOBCARBON	L3JRC
ORC-err-burn	28	–	–	–
ORC-err-noburn	–	27	56	90
ORC-good	88	130	70	94
ORC-max	181	28	21	28
ORC-min	32	158	140	173
Global (Total)	329	344	287	384

## Modelling global burned area and fire regime

C. Yue et al.

**Table 2.** Model error characterization in comparison with the GFED3.1 data for 1997–2009.  $E_{BA}$ , the model error of mean annual burned area in relative to the GFED3.1 data;  $S_{interannual}$ , the correlation coefficient of linearly detrended monthly simulated and GFED3.1 burned area series;  $S_{season}$ , the seasonal similarity of burned area by the model and the GFED3.1 data (see Sect. 2.5 for more detailed information).

Region (in Fig. 2a)	$E_{BA}$	$S_{interannual}$	$S_{season}$	Burned area by GFED3.1 ( $\text{hayr}^{-1}$ )	Percentage of the global total burned area (GFED3.1)	Percentage of the global total burned area (ORCHIDEE)	Peak fire month (GFED3.1, model)
BONA	0.6	0.70	0.71	2.1	0.6	1.0	(7,7)
TENA	19	0.63	0.76	1.3	0.4	8.0	(8,7)
CEAM	4.0	0.53	0.64	1.2	0.3	1.8	(5,4)
NHSA	3.0	0.79	0.96	2.1	0.6	2.7	(2,2)
SHSA	1.6	0.65	0.71	19	5.5	15.7	(9,8)
EURO	5.2	0.63	0.86	0.4	0.1	0.7	(8,8)
MIDE	38	0.60	0.73	0.4	0.1	5.5	(8,6)
NHAF	-0.4	0.50	0.57	125	35.7	24.3	(12,12)
SHAF	-0.6	0.62	0.68	123	35.2	14.0	(8,6)
BOAS	-0.1	0.38	0.55	5.5	1.6	1.6	(7,7)
CEAS	3.7	0.56	0.75	11	3.0	15.8	(8,7)
SEAS	0.3	0.24	0.50	4.6	1.3	1.9	(3,4)
EQAS	-0.8	0.85	0.72	1.7	0.5	0.1	(9,9)
AUST	-0.6	0.51	0.65	52	15.0	6.8	(10,11)

Title Page

Abstract

Introduction

Conclusions

References

Tables

Figures

⏪

⏩

◀

▶

Back

Close

Full Screen / Esc

Printer-friendly Version

Interactive Discussion



## Modelling global burned area and fire regime

C. Yue et al.

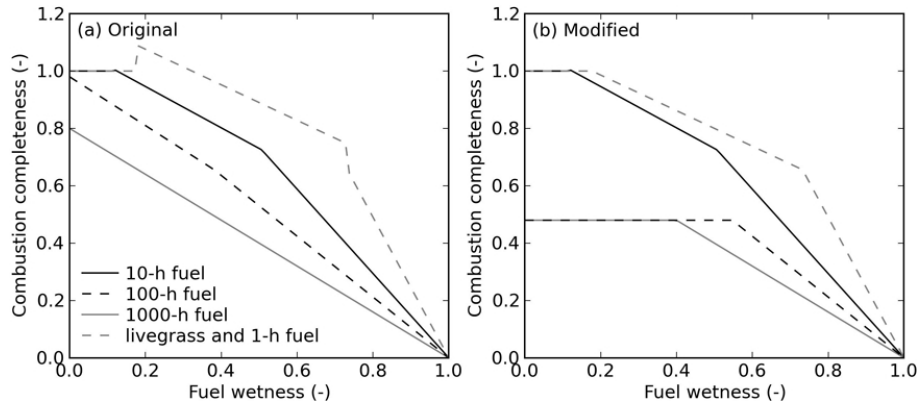


**Fig. 1.** Surface-fuel combustion fraction as a function of fuel wetness in **(a)** the original SPIT-FIRE model by Thonicke et al. (2010) and **(b)** as modified in the present study, taking the tropical forests as an example. The combustion of live grass biomass is assumed to follow the same as the 1-h dead fuel.

Title Page

Abstract

Introduction

Conclusions

References

Tables

Figures

◀

▶

◀

▶

Back

Close

Full Screen / Esc

Printer-friendly Version

Interactive Discussion



## Modelling global burned area and fire regime

C. Yue et al.

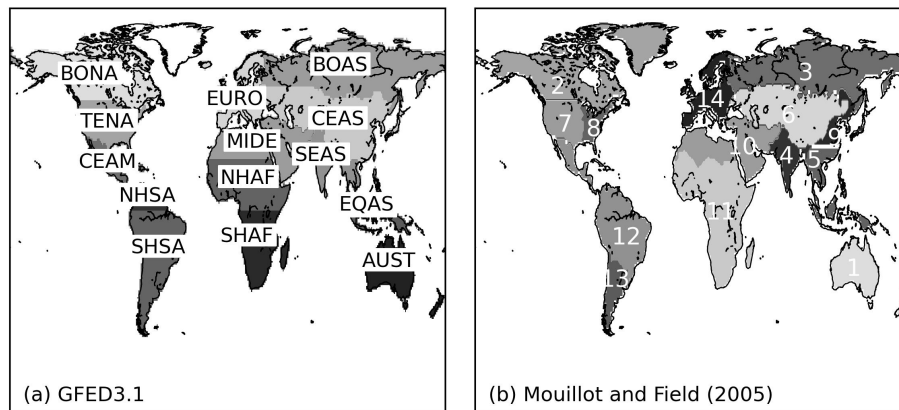


**Fig. 2.** The regional breakup of the globe for **(a)** the GFED3.1 dataset: BONA, Boreal North America; TENA, Temperate North America; CEAM, Central America; NHSA, Northern Hemisphere South America; SHSA, Southern Hemisphere South America; EURO, Europe; MIDE, Middle East; NHAF, Northern Hemisphere Africa; SHAF, Southern Hemisphere Africa; BOAS, Boreal Asia; CEAS, Central Asia; SEAS, Southeast Asia; EQAS, Equatorial Asia; AUST, Australia and New Zealand. And **(b)** by Mouillot and Field (2005): (1) Australia and New Zealand; (2) Boreal North America; (3) Boreal Russia; (4) India; (5) South East Asia; (6) Central Asia; (7) USA (West Mississippi); (8) USA (East Mississippi); (9) East Asia; (10) Middle East and Northern Africa; (11) Africa (sub-Saharan); (12) Central South America; (13) Southern South America; (14) Europe.

Title Page

Abstract

Introduction

Conclusions

References

Tables

Figures

◀

▶

◀

▶

Back

Close

Full Screen / Esc

Printer-friendly Version

Interactive Discussion



## Modelling global burned area and fire regime

C. Yue et al.

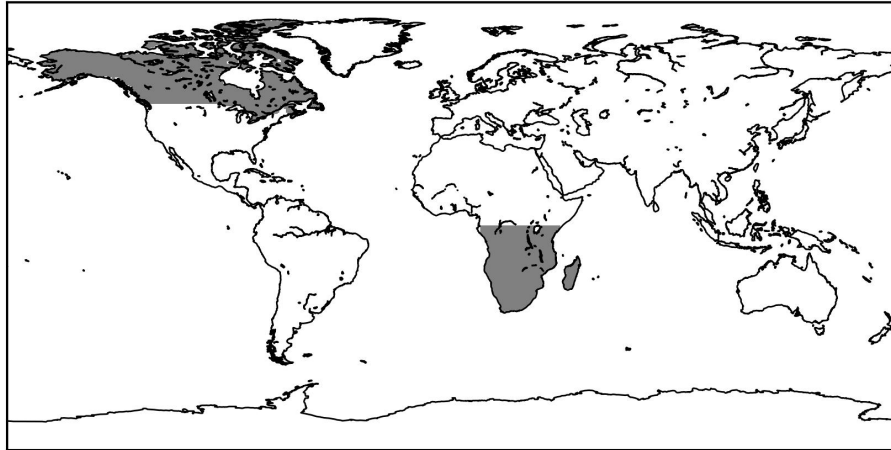


**Fig. 3.** Spatial extent of the fire data used in the two case studies on fire size distribution for boreal North America and the southern Africa.

[Title Page](#)[Abstract](#)[Introduction](#)[Conclusions](#)[References](#)[Tables](#)[Figures](#)[⏪](#)[⏩](#)[◀](#)[▶](#)[Back](#)[Close](#)[Full Screen / Esc](#)[Printer-friendly Version](#)[Interactive Discussion](#)

## Modelling global burned area and fire regime

C. Yue et al.

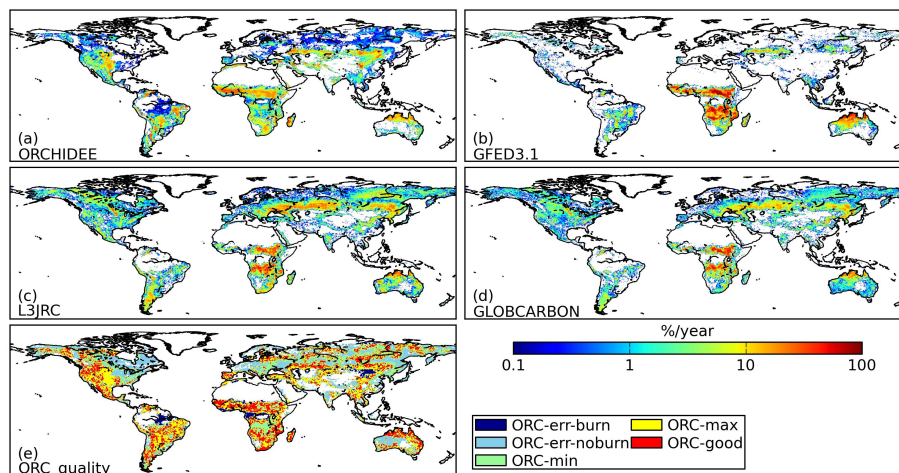


**Fig. 4.** Mean annual burned fraction (in percentage) over 2001–2006 **(a)** as simulated by ORCHIDEE, and by the satellite-derived burned area datasets: **(b)** GFED3.1, **(c)** L3JRC and **(d)** GLOBCARBON. The subplot **(e)** shows for each grid cell the quality flag of the ORCHIDEE-simulated burned fraction in comparison with the three observation datasets. ORC-err-burn, where ORCHIDEE shows burning but the other three observation datasets do not; ORC-err-noburn, where at least two out of the three observation datasets do show burning, but ORCHIDEE does not; ORC-min, where ORCHIDEE simulates lower burned fraction than the other three datasets; ORC-max, where ORCHIDEE simulates higher burned fraction; ORC-good, where ORCHIDEE-simulated burned fraction falls within the range given by the other three datasets. When calculating the minimum and maximum burned fraction of the three observation datasets, an arbitrary tolerance margin of 25% was applied around the min/max value to take into account the uncertainty of the observation data.

Title Page

Abstract

Introduction

Conclusions

References

Tables

Figures

◀

▶

◀

▶

Back

Close

Full Screen / Esc

Printer-friendly Version

Interactive Discussion



## Modelling global burned area and fire regime

C. Yue et al.

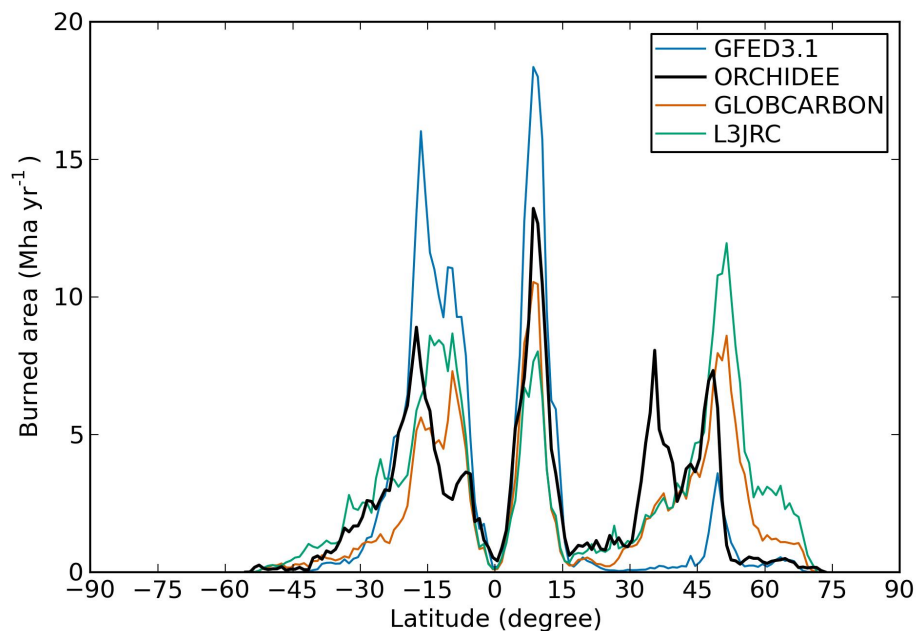


**Fig. 5.** The latitudinal distribution of burned area ( $\text{Mha yr}^{-1}$ ) according to GFED3.1 (blue), ORCHIDEE (thick black), GLOBCARBON (orange) and L3JRC (green). Data are shown for the mean annual value for 2001–2006.

[Title Page](#)[Abstract](#)[Introduction](#)[Conclusions](#)[References](#)[Tables](#)[Figures](#)[◀](#)[▶](#)[◀](#)[▶](#)[Back](#)[Close](#)[Full Screen / Esc](#)[Printer-friendly Version](#)[Interactive Discussion](#)

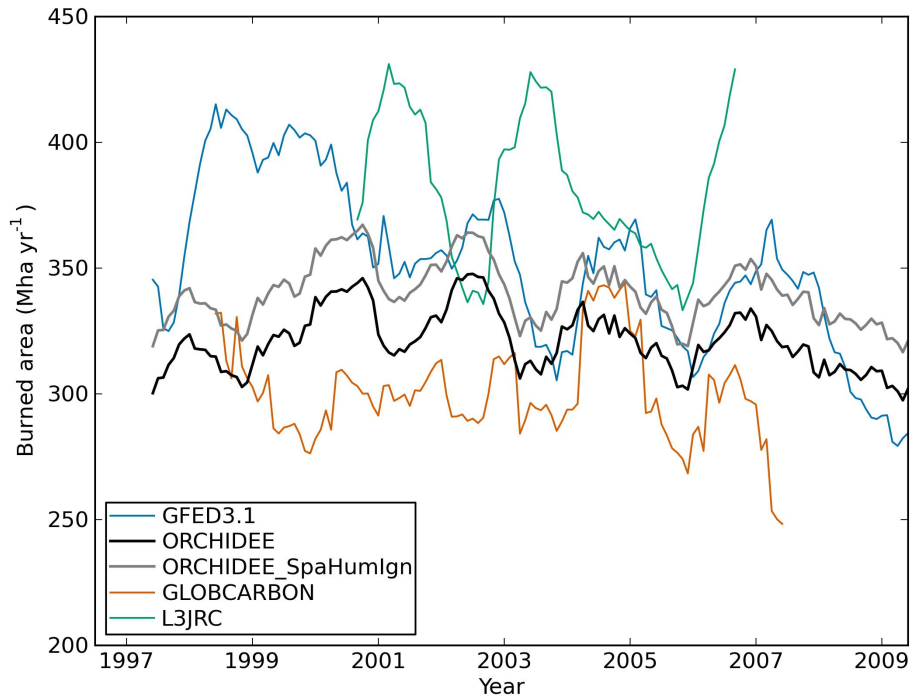


**Fig. 6.** Twelve-month running means of total global burned area ( $\text{Mha yr}^{-1}$ ) according to GFED3.1 (blue), ORCHIDEE simulation (black), ORCHIDEE simulation with spatial  $a(\text{ND})$  dataset in human ignition (grey), GLOBCARBON (orange) and L3JRC (green).

**Modelling global burned area and fire regime**

C. Yue et al.

[Title Page](#)

[Abstract](#)   [Introduction](#)

[Conclusions](#)   [References](#)

[Tables](#)   [Figures](#)

[◀](#)   [▶](#)

[◀](#)   [▶](#)

[Back](#)   [Close](#)

[Full Screen / Esc](#)

[Printer-friendly Version](#)

[Interactive Discussion](#)



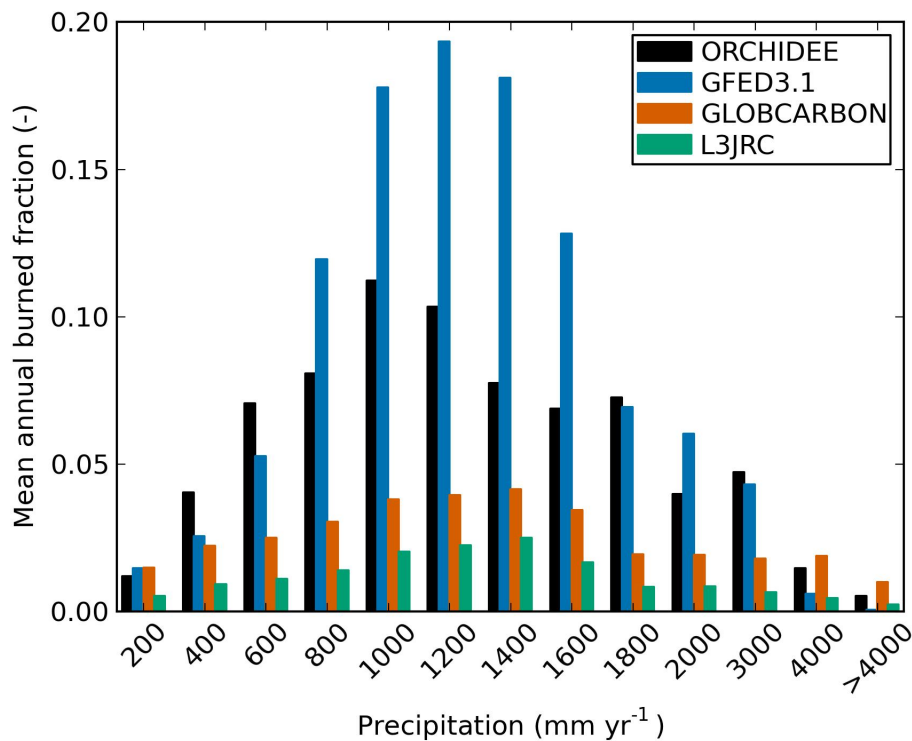


**Fig. 7.** Burned fraction distribution as a function of annual precipitation according to: the model simulation (black), GFED3.1 (blue), GLOBCARBON (orange) and L3JRC (green) data for the tropical and subtropical regions (35° S–35° N). The annual precipitation data are from CRU data and binned in 200 mm intervals.

Modelling global burned area and fire regime

C. Yue et al.

Title Page

Abstract Introduction

Conclusions References

Tables Figures

◀ ▶

◀ ▶

Back Close

Full Screen / Esc

Printer-friendly Version

Interactive Discussion



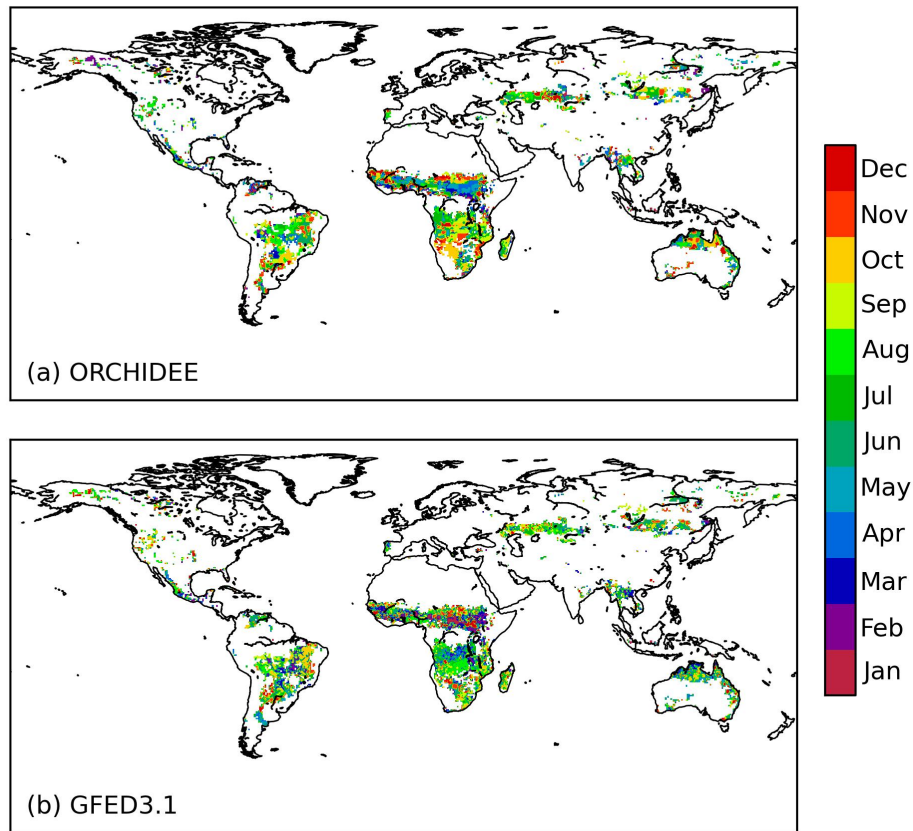


**Fig. 8.** Spatial pattern of the peak fire month by **(a)** ORCHIDEE simulation and **(b)** GFED3.1 data over the period of 1997–2009. Only regions with fire collocated in both datasets are shown.

Modelling global burned area and fire regime

C. Yue et al.

Title Page

Abstract

Introduction

Conclusions

References

Tables

Figures

◀

▶

◀

▶

Back

Close

Full Screen / Esc

Printer-friendly Version

Interactive Discussion



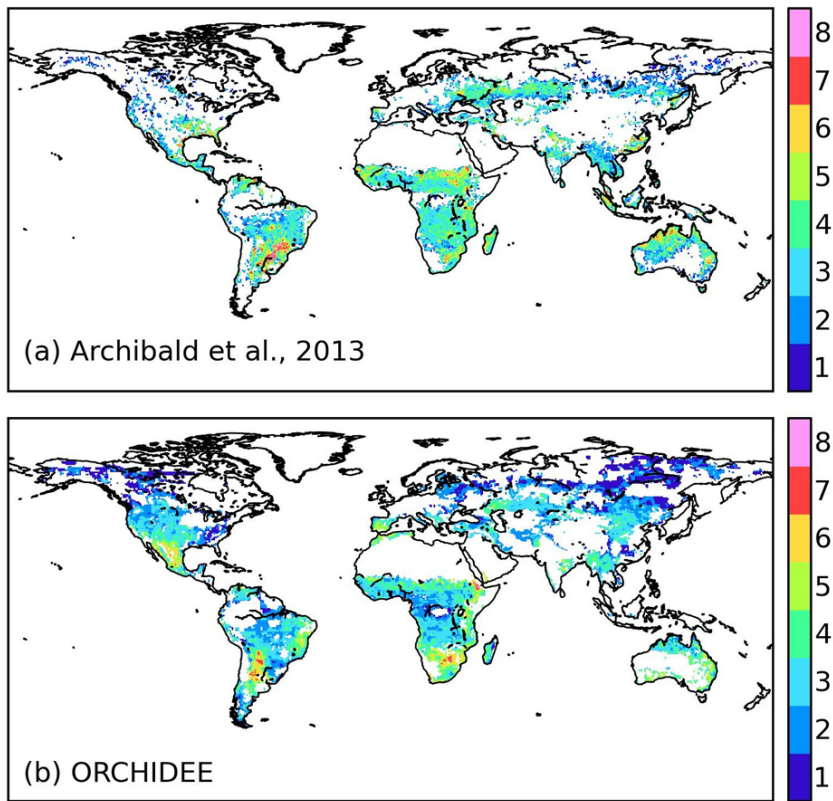


**Fig. 9.** Fire season length (months) by (a) Archibald et al. (2013) derived from GFED3.1 data, and (b) ORCHIDEE simulation for the period of 1997–2009.

**Modelling global  
burned area and fire  
regime**

C. Yue et al.

Title Page

Abstract Introduction

Conclusions References

Tables Figures

◀ ▶

◀ ▶

Back Close

Full Screen / Esc

Printer-friendly Version

Interactive Discussion



## Modelling global burned area and fire regime

C. Yue et al.

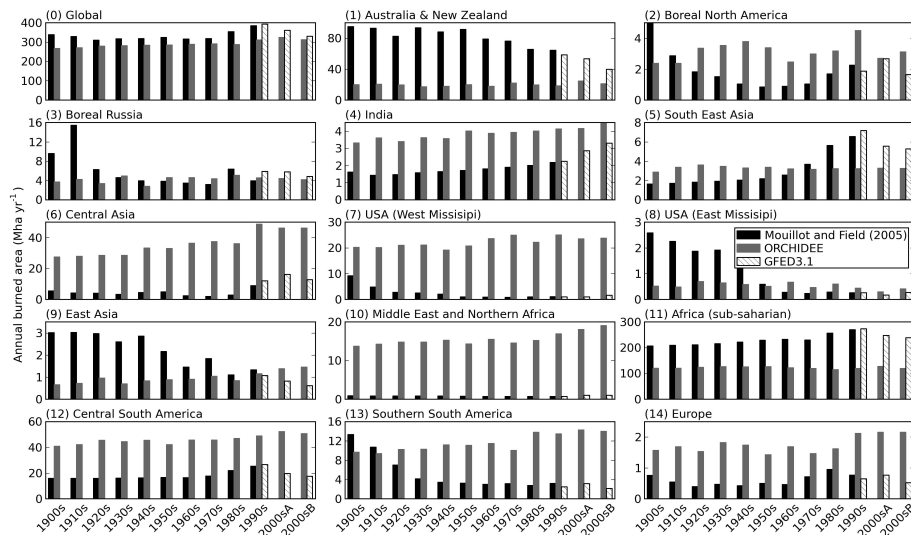


**Fig. 10.** The annual burned area for 1901–2009 as simulated by ORCHIDEE (grey bar), reported by the Mouillot data (Mouillot and Field, 2005, black bar), and by GFED3.1 data (dashed white bar). Data are shown for the mean values over each decade for 1901–2000, and for 2001–2005 (2000sA) and 2006–2009 (2000sB). Refer to Sect. 2.4.1 for the correction of the Mouillot data by using GFED3.1 data.

Title Page

Abstract

Introduction

Conclusions

References

Tables

Figures



Back

Close

Full Screen / Esc

Printer-friendly Version

Interactive Discussion



## Modelling global burned area and fire regime

C. Yue et al.

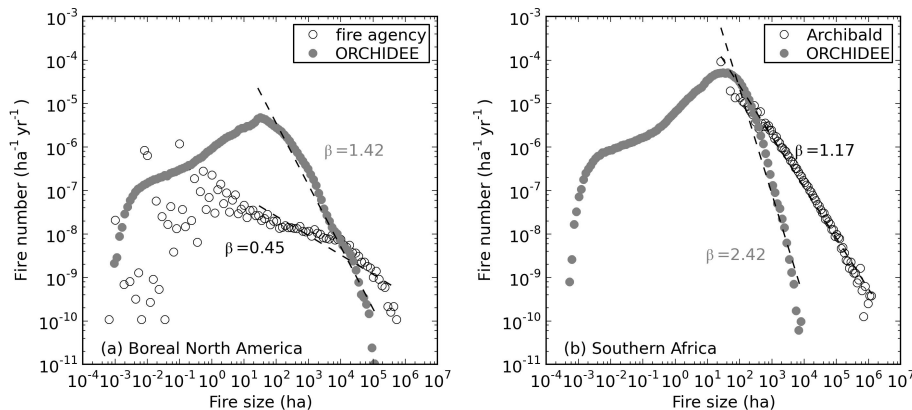


**Fig. 11.** Fire size distribution as simulated by the model and derived from (a) fire management agency statistical data for Canada and Alaska (boreal North America), and (b) MODIS 500 m burned area data by Archibald et al. (2010) for southern Africa. The horizontal axis indicates fire size (ha) and the vertical axis indicates the corresponding number of fires (in units of  $\text{ha}^{-1} \text{yr}^{-1}$ ) for the given fire size.

Title Page

Abstract

Introduction

Conclusions

References

Tables

Figures

◀

▶

◀

▶

Back

Close

Full Screen / Esc

Printer-friendly Version

Interactive Discussion





### 95th quantile fire size

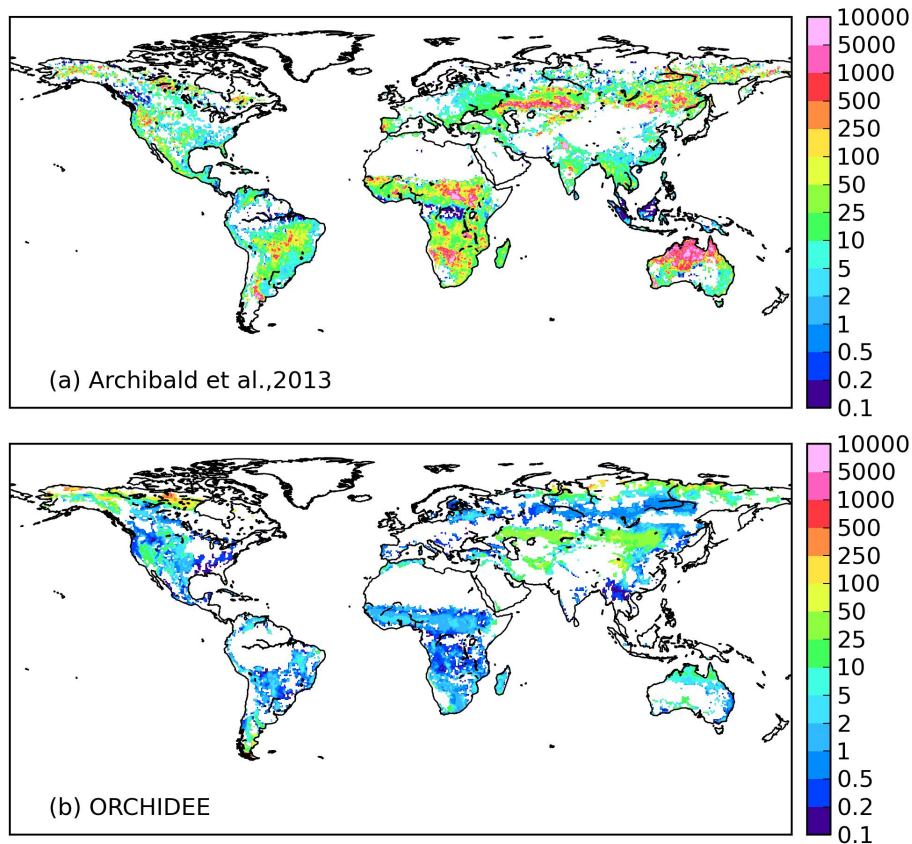


**Fig. 13.** Map of the 95th quantile fire size ( $\text{km}^2$ ) as given by **(a)** Archibald et al. (2013) from MCD45A1 MODIS 500 m burned area data, and **(b)** ORCHIDEE simulation.

## Modelling global burned area and fire regime

C. Yue et al.

Title Page

Abstract

Introduction

Conclusions

References

Tables

Figures

◀

▶

◀

▶

Back

Close

Full Screen / Esc

Printer-friendly Version

Interactive Discussion



## Modelling global burned area and fire regime

C. Yue et al.

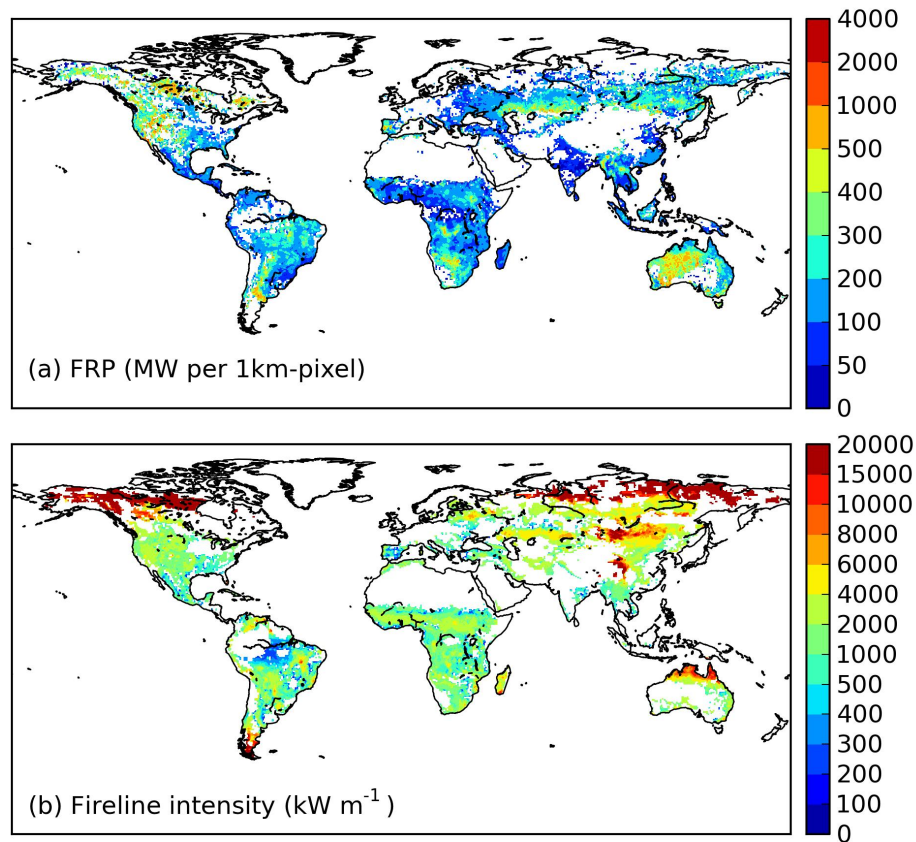


**Fig. 14.** Comparison of the spatial pattern of observed and simulated fire intensity. **(a)** The 95th quantile fire radiative power (FRP, in unit of MW per 1 km-pixel) as derived by Archibald et al. (2013) from the MODIS FRP data. **(b)** Fireline intensity as simulated by ORCHIDEE.

[Title Page](#)[Abstract](#)[Introduction](#)[Conclusions](#)[References](#)[Tables](#)[Figures](#)[◀](#)[▶](#)[◀](#)[▶](#)[Back](#)[Close](#)[Full Screen / Esc](#)[Printer-friendly Version](#)[Interactive Discussion](#)